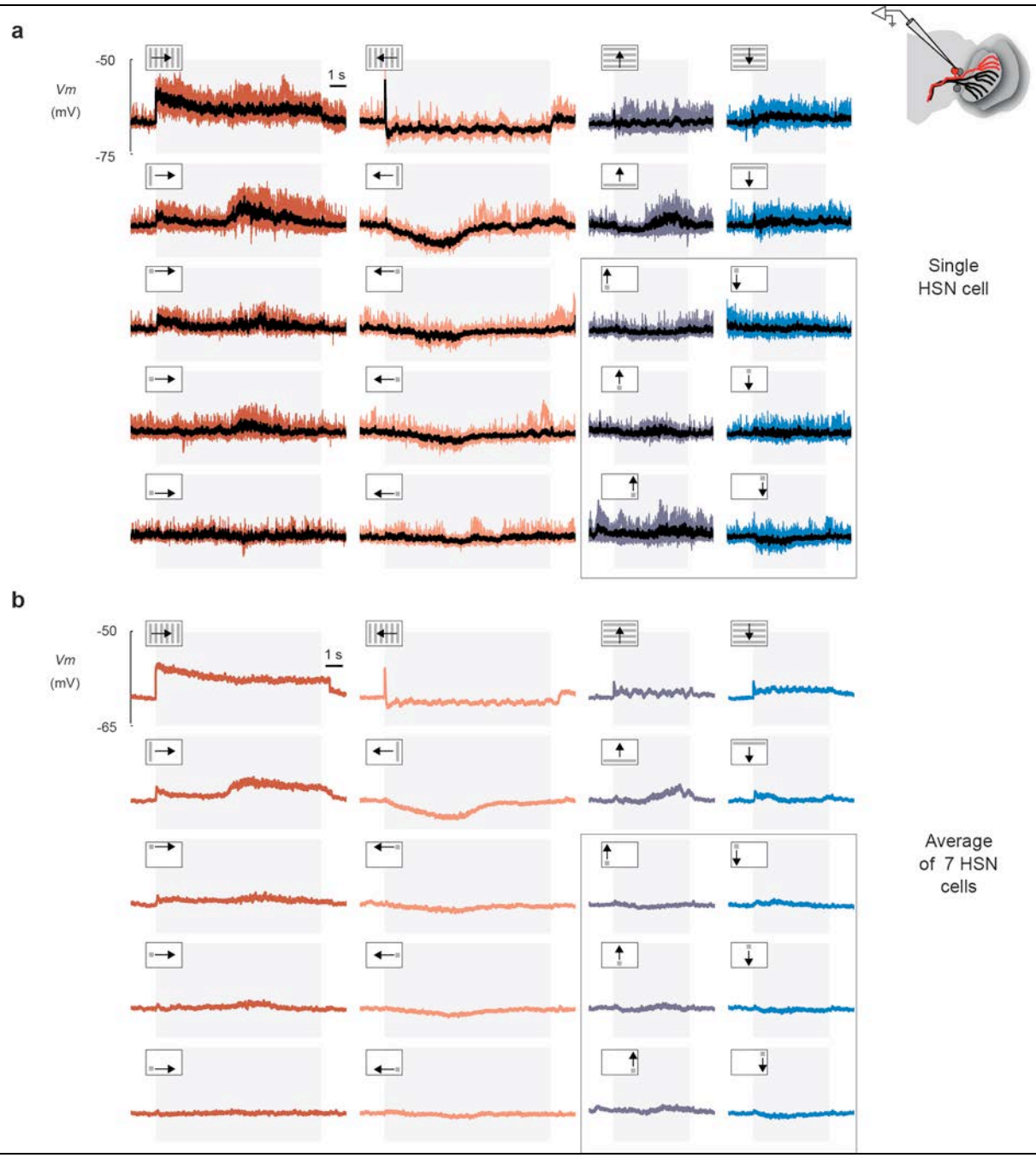

Supplementary Figure 1

Horizontal System North (HSN) cells respond best, and in a direction-selective manner, to horizontally moving gratings or long bars.

(a) Responses of a single HSN cell, recorded in the right lobula plate, to gratings, long bars, and small spots moving in four directions. Single trials are shown in color and the average responses are shown in black (5-6 trials per condition). The gratings had a spatial wavelength of 18 ˚/cycle and a temporal frequency of 1.25 cycles / s. Bars (9˚ wide x 75˚ high) and spots (9˚ x 9˚) moved at 22.5˚/s. (b) Averaged responses of 7 HSN cells, all recorded in the right lobula plate.

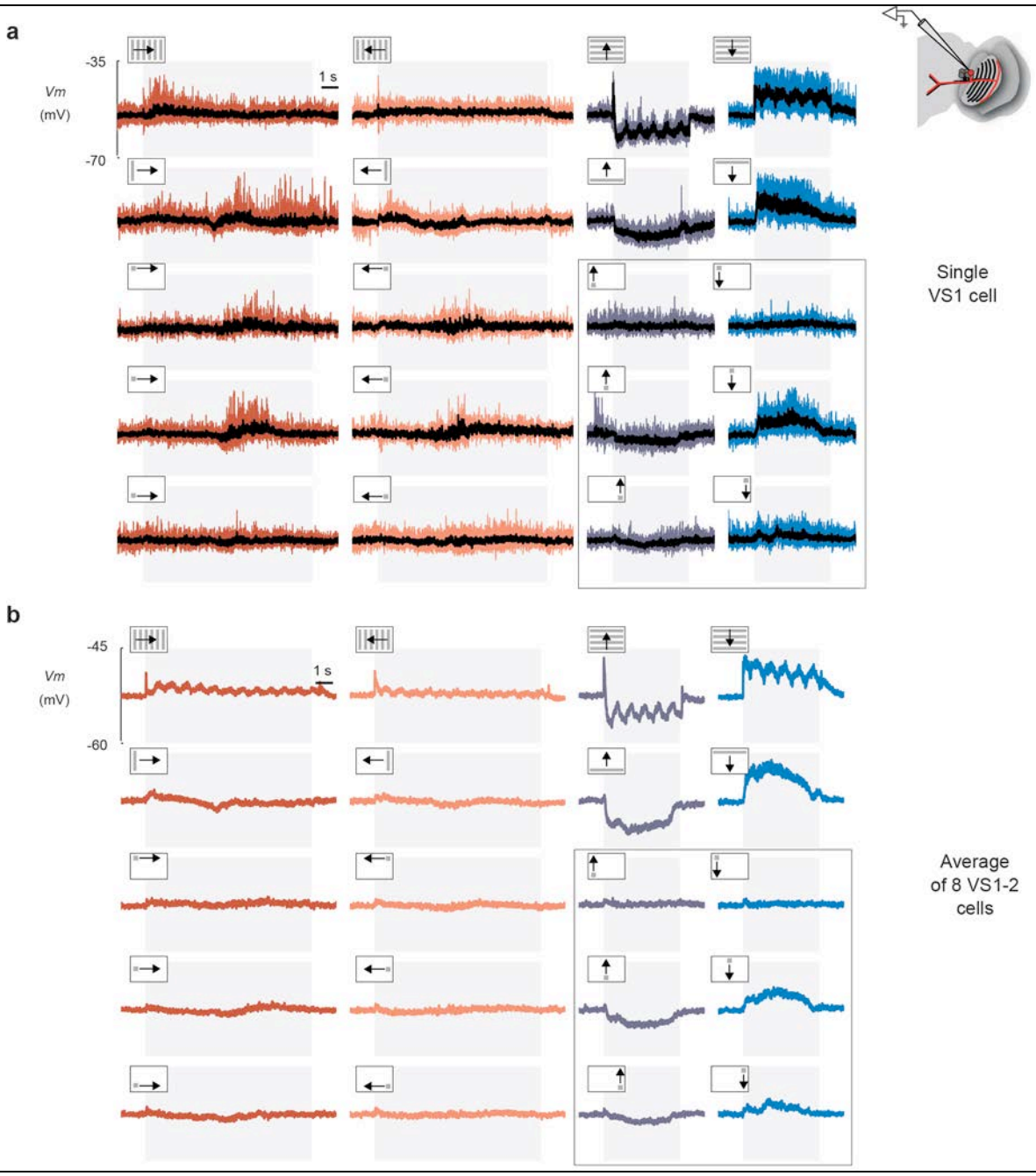

Supplementary Figure 2

Vertical System (VS) 1-2 cells respond best, and in a direction-selective manner, to vertically moving gratings or long bars.

(a) Responses of a single VS1 cell, recorded in the right lobula plate, to gratings, long bars, and small spots moving in four directions. Single trials are shown in color and the average responses are shown in black (5-6 trials per condition). The gratings had a spatial wavelength of 18 ˚/cycle and a temporal frequency of 1.25 cycles / s. Bars (9˚ wide x 75˚ high) and spots (9˚ x 9˚) moved at 22.5˚/s. (b) Averaged responses of 8 VS1-2 cells, all recorded in the right lobula plate.

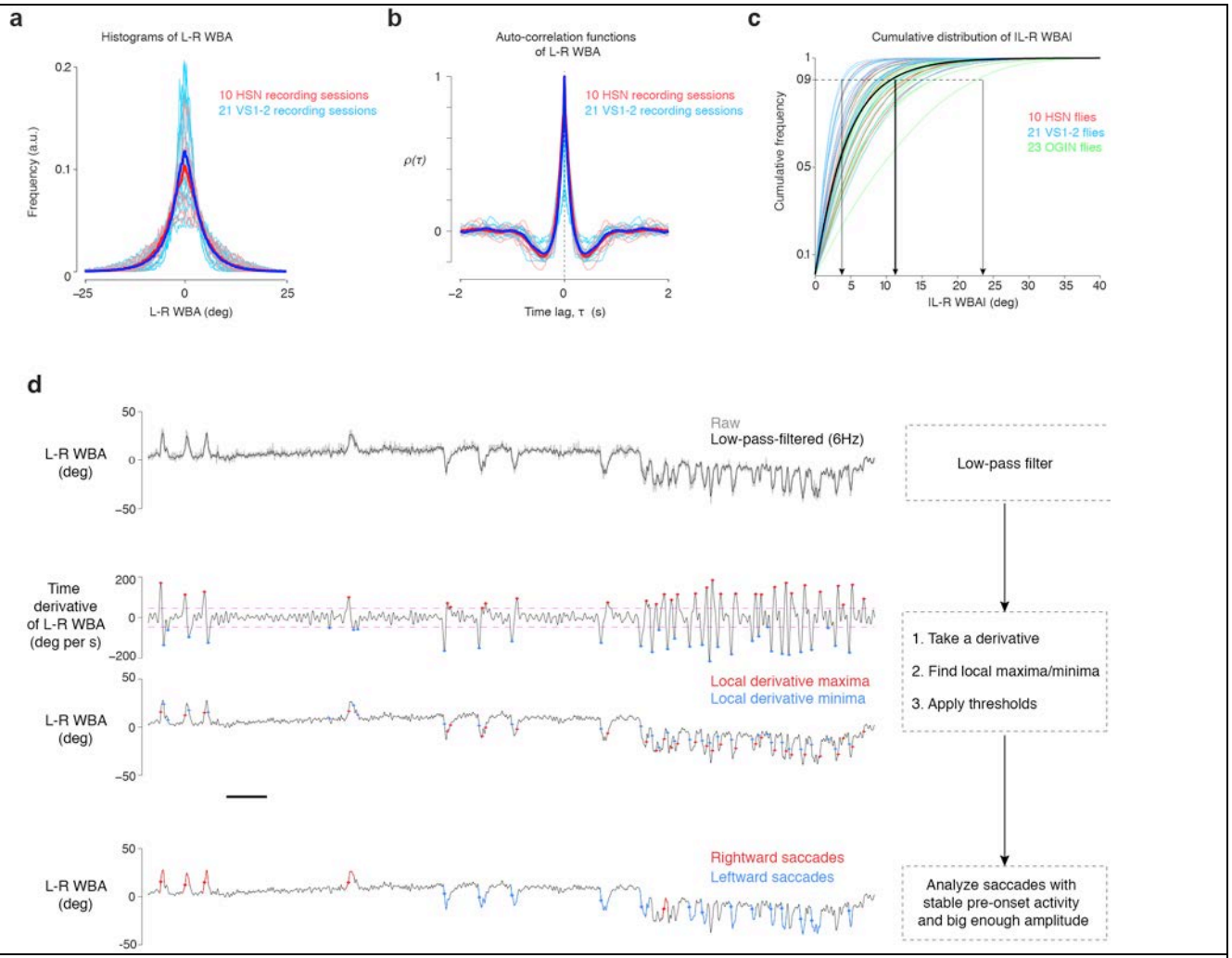

Supplementary Figure 3

Visualizing wingstroke amplitude statistics and an explanation of how we detect saccades

(a) Histograms of L-R WBA from 10 recording sessions with HSN cells (red) and 21 sessions with VS1-2 cells (blue). Light lines represent histograms from individual flies and the dark lines are averages across flies. The L-R WBA signal was high-pass-filtered before computing histograms, to eliminate slow drift. (b) Auto-correlation functions of L-R WBA for the same set of cells, depicted in the same color scheme as in panel a. (c) Cumulative distribution functions (cdfs) of L-R WBA for all flies studied. L-R WBA was high-pass filtered with a 1 Hz cut-off before plotting cdfs so as to eliminate slow drift in the L–R WBA trace. To get further analyzed, putative saccades had to cross an amplitude threshold in the last step of the saccade detection algorithm. This amplitude threshold was set at the 90th percentile of the L-R WBA cdf from that session (thin arrows indicate the smallest and largest thresholds used; thick arrow indicates the mean threshold used across all sessions). (d) Detecting saccades in a sample trace. Top row: a sample L-R WBA trace (gray) and a low-pass filtered version (6 Hz cut-off frequency) are shown. Second row: the derivative of the low-pass-filtered L-R WBA is shown, with putative rightward saccades marked by red dots and putative leftward saccades marked by blue dots. Putative saccades were detected from local maxima and minima in the L-R WBA derivative trace whose magnitude exceeded a positive or negative threshold (magenta lines), respectively. Third row: putative saccades are shown as red and blue dots on the low-pass filtered L-R WBA trace. Bottom row: same as the third row except we highlight saccades that were analyzed further in this manuscript by coloring the L–R WBA trace—red for rightward saccades; blue for leftward saccades—to indicate the onset moment, end moment, and duration of each analyzed saccade. To be analyzed, saccades had to cross an amplitude threshold, described in panel c, and also had to have a stable L–R WBA signal prior to saccade onset, so that we could assign a clear onset time to the saccade (Online Methods).

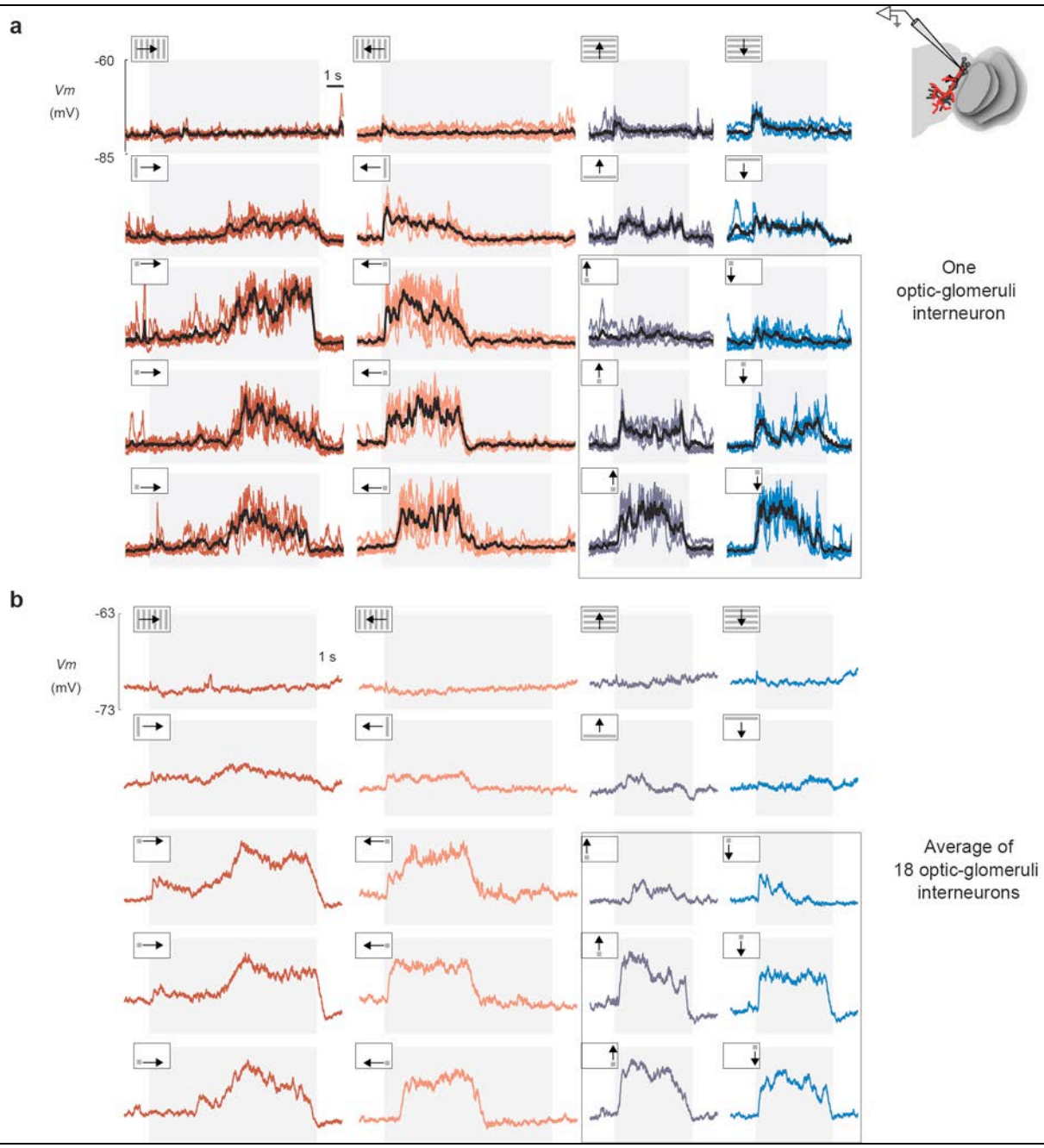

Supplementary Figure 4

Optic-glomeruli interneurons (OGINs) respond best to small spots, in a non-directional manner, and only weakly to long bars or gratings.

(a) Responses of a single OGIN, recorded in the right half of the brain, to gratings, long bars, and small spots moving in four directions. Single trials are shown in color and the average responses are shown in black (5-6 trials per condition). The gratings had a spatial wavelength of 18 ˚/cycle and a temporal frequency of 1.25 cycles / s. Bars (9˚ wide x 75˚ high) and spots (9˚ x 9˚) moved at 22.5˚/s. (b) Average responses of 18 OGINs recorded on the right side of the brain. Out of 21 spot-selective OGINs analyzed in Figure 5, three cells were excluded in this analysis because we did not maintain the recording long enough to obtain complete receptive field measurements. (Note that all 21 cells in Figure 5 were tested with a reduced set of stimuli, early in the recording session, which were sufficient to determine spot selectivity and receptive-field width.)

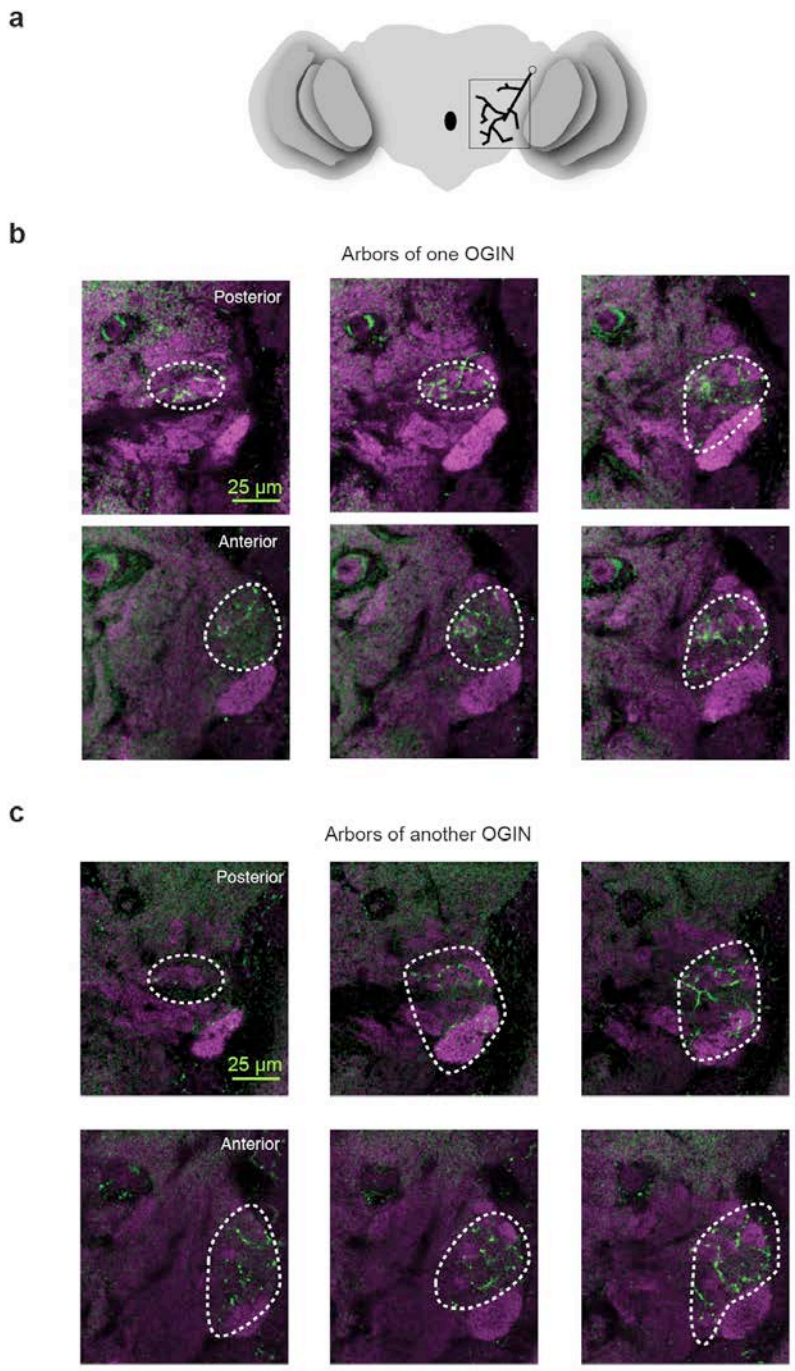

Supplementary Figure 5

Optic-glomeruli interneurons (OGINs) arborize in the lateral protocerebrum.

These representative images illustrate the anatomy of the recorded neurons. (a) Schematic of an OGIN. Black box highlights the region shown in panels b and c. (b) Six z-slices of a filled OGIN in the right hemisphere, 5 µm spacing. Z-slices are arranged clockwise from posterior or neuraxis dorsal (closer to the protocerebral bridge) to anterior or neuraxis ventral (closer to the antennal lobe.). Immunoamplified neuropil signal is shown in magenta (nc82 anti-Bruchpilot antibody) and biocytin filled neurites in green. The GFP channel is not shown.) Dashed circles highlight regions with neurite arborizations. (c) Same as in panel b, but for a second cell.

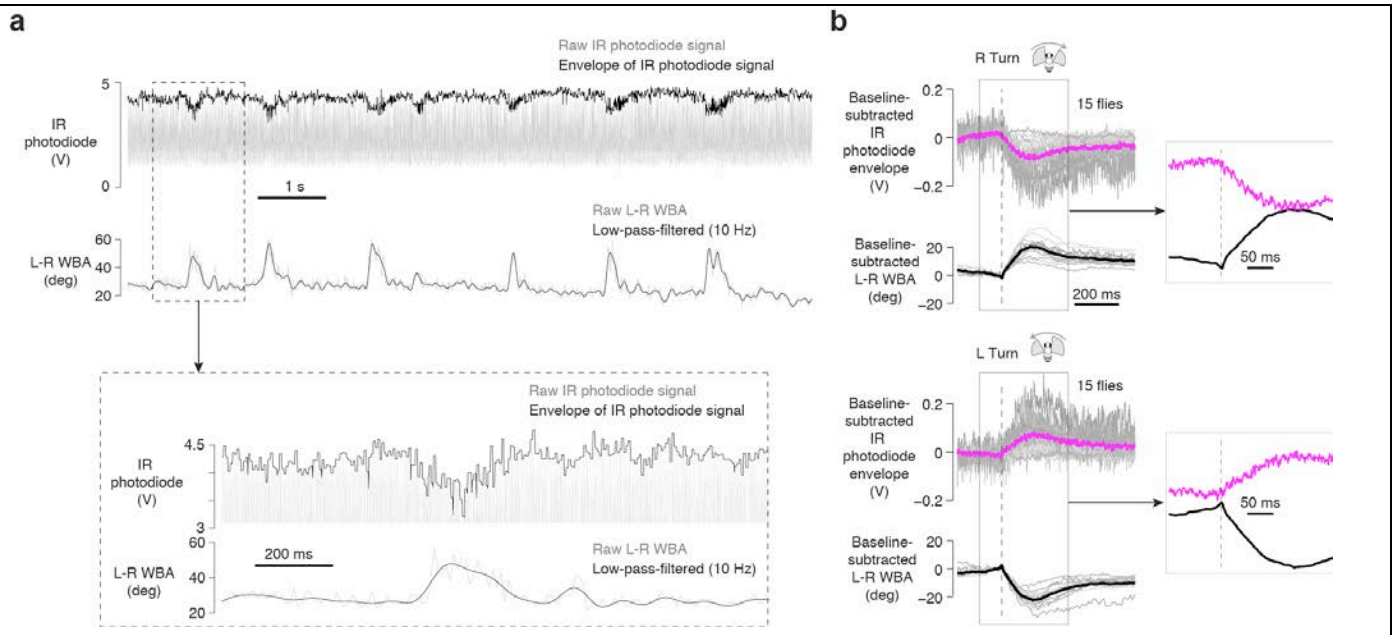

Supplementary Figure 6

An IR photodiode signal to monitor wingbeat motion confirms the precision of the video-based analysis of saccade onset times.

(a) A photodiode placed beneath the fly's left wing showed oscillations in its signal as the wing swept back and forth during each wingstroke. While the shape and magnitude of the photodiode signal were not calibrated to any specific kinematic parameter of the wing's trajectory, we noticed that the envelope of the signal changed amplitude briefly with each saccade. Thus, the photodiode signal could provide a second measure of the onset times of saccades, beyond the estimate derived from analyzing video images. We calculated the maximum of the photodiode trace in a 6-ms sliding-window, which generated an envelope signal. (6 ms is slightly longer than the longest inter-wingstroke interval.) Saccades were clearly evident in this envelope signal as negative deviations for rightward saccades (shown here) and positive deviations for leftward saccades (shown in panel b). (b) Average photodiode and L–R WBA traces associated with saccades for 15 flies. Saccades were culled from the L–R WBA trace (Online Methods and Supplementary Figure 3). Individual-fly averages are shown in gray. Averages across experiments are shown in magenta or black. Insets show the same traces at a higher temporal resolution.

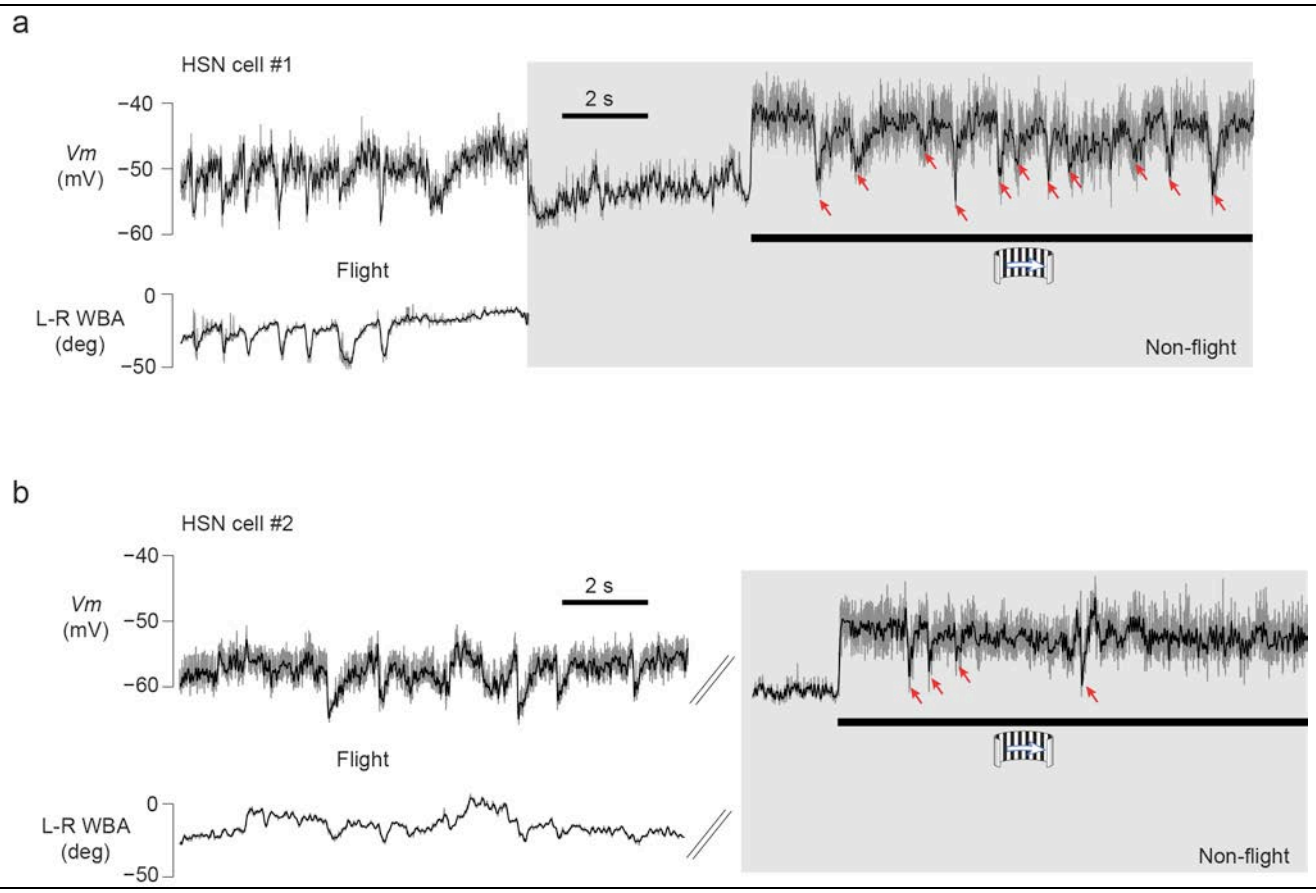

Supplementary Figure 7

We observed, during non-flight, examples where the HSN membrane potential was dynamically modulated in a manner that resembled saccade related potentials.

(a) The membrane potential (*Vm*) of a single HSN cell during flight and immediately after the fly stopped flying. After the cessation of flight, we observed SRP-like changes in *Vm* (red arrows), which were most obvious during a presentation of a grating moving in the cell's preferred direction. The unfiltered *Vm* is shown in gray and a low-pass filtered version (20-Hz cut-off) is shown in black. The unfiltered L–R WBA is shown in gray and a low-pass filtered version (10-Hz cut-off) is shown in black. (b) Same as in panel a for a second HSN cell. The non-flight trace in this example starts ~10 s after the cessation of flight. These example traces suggest that SRPs in HSN cells do not require flight-associated wing movements.

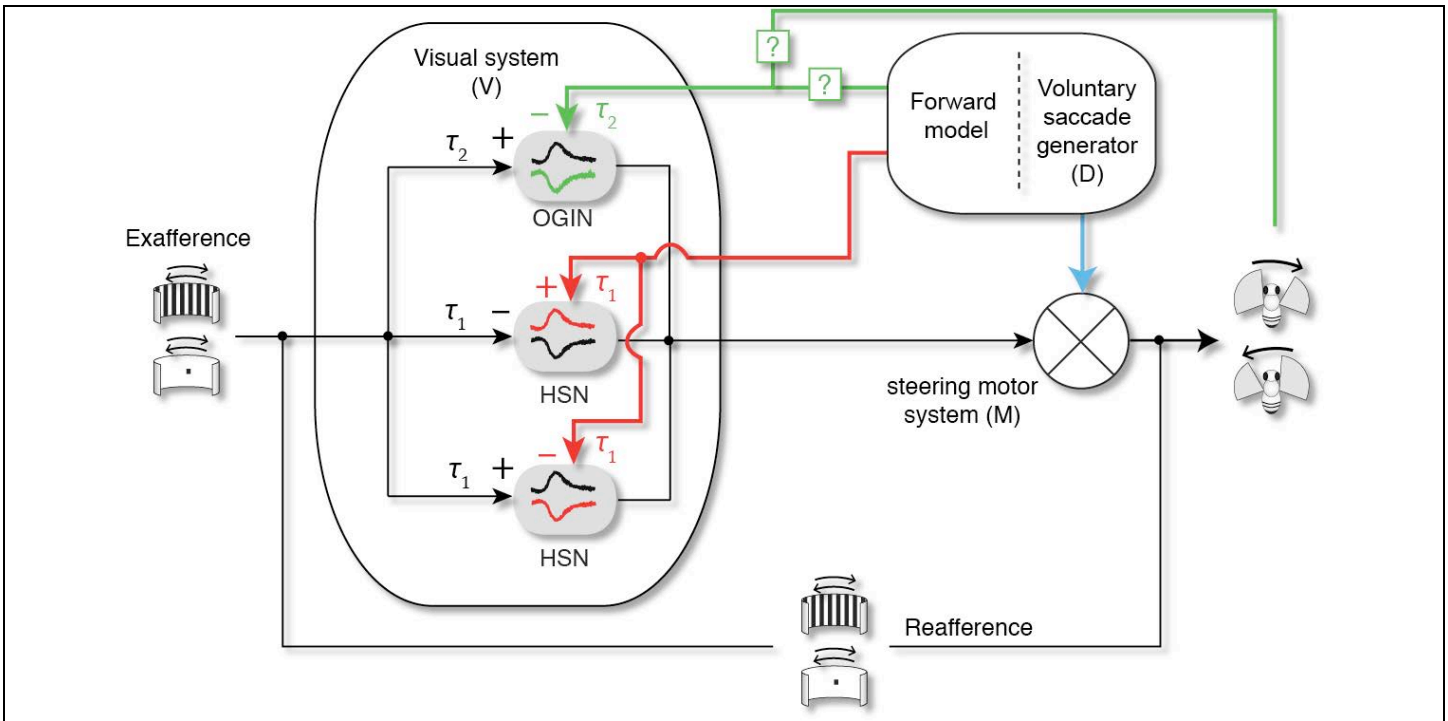

Supplementary Figure 8

Summary diagram of motor-related silencing of visual neurons in *Drosophila*.

A command to perform a saccade is generated by a hypothesized voluntary saccade generator. This command is sent to the flight motor system (blue line). The sensory consequences of the command are internally computed by a putative forward model of unknown complexity and these predictions are sent to the visual system (red and green lines). Visual neurons receive motor related inputs (red and green arrows) that oppose the expected reafferent visual input from the saccade. Black τ_n's represent the visual response latency of each cell. Red and green τ_n's represent the latency of motor-related inputs to each cell, which are tailored to the visual response latency. Because saccadic motor-related inputs to OGINs arrive 69-70 ms after the wings move, it is possible that the motor related signals to these cells originate as a sensory, perhaps mechanosensory, feedback from the act of turning; we indicate the possibility of OGIN silencing arising from either sensory feedback or an internal/forward model by the two question marks overlaying green lines that indicate the two possible feedback routes.

	HSN cell visual response (Leftward moving grating)	HSN cell SRP (Right turns)	**HSN cell visual response (Rightward moving grating)**	HSN cell SRP (Left turns)	**OGIN visual response (Leftward moving spot)**	OGIN SRP (Right turns)	**OGIN visual response (Rightward moving spot)**	OGIN SRP (Left turns)
min/max of the baseline interval	30 ms	-25 ms	24 ms	-39 ms	51 ms	68 ms	51 ms	69 ms
mean ± 2SD of the baseline interval	29 ms	-25 ms	23 ms	-21 ms	51 ms	68 ms	49 ms	72 ms
mean ± 1SD of the baseline interval	24 ms	-46 ms	22 ms	-40 ms	49 ms	67 ms	48 ms	66 ms

Supplementary Table 1. The neuronal latencies estimated in Figure 6 are not strongly changed by the threshold criterion used to estimate response onsets. We detected the onset latencies of average visual responses and SRPs in Fig. 6d and 6e using a simple algorithm described in the Online Methods. In short, we found the maximum and minimum *Vm* or L–R WBA value in a baseline time window for each curve. These maximum and minimum values were considered thresholds. Starting at the peak response for each curve, we moved backward in time and called the point in time at which the *Vm* or L–R WBA curve crossed either of these thresholds, whichever came first, the onset latency. The results of this algorithm are shown as the top row in the table (and in Fig. 6d and 6e). For rows 2 and 3, we measured the mean and standard deviation (SD) of the data points in the baseline period, and considered the values at ±1 SD or ±2 SD as thresholds. The latencies calculated with the same algorithm, but using these thresholds, are shown in rows 2 and 3.